

Jet-Flavor Tagging Performance at FCC-ee

Sara Aumiller^{1*}, Dolores Garcia^{2*} and Michele Selvaggi^{2*}

¹Technical University of Munich (TUM), Munich, Germany.

²CERN, Geneva, Switzerland.

*Corresponding author(s). E-mail(s): sara.aumiller@cern.ch;
dolores.garcia@cern.ch; michele.selvaggi@cern.ch;

1 Introduction

A jet can be viewed as an ensemble of particles originating from the same source. The source can either be a quark, gluon, or even a hadronically decaying τ lepton, which hadronizes and creates a narrow cone of traceable particles in the detector. Determining the particle type of the jet origin is referred to as jet-flavor tagging.

At future Higgs factories like FCC-ee, we are particularly interested in precision measurements of the Higgs bosons such as the determination of the branching ratios to fermions and their couplings. Jet-flavor tagging is indispensable to perform these measurements. However, this has only been performed on the IDEA detector on fast simulation so far [1]. To address this, we implement jet-flavor tagging for the CLD detector, evaluating its tagging performance on fast and, for the first time at FCC-ee, full simulation.

1.1 Jet-flavor tagging set-up

To study jet-flavor tagging at FCC-ee, we use the process of $e^+e^- \rightarrow Z \rightarrow ZH$ at 240 GeV with the Higgs boson decaying into two jets $H \rightarrow jj$ that we will study. For simplicity, we let the Z boson decay into two neutrinos $Z \rightarrow \nu\bar{\nu}$. This leaves two jets as an event signature.

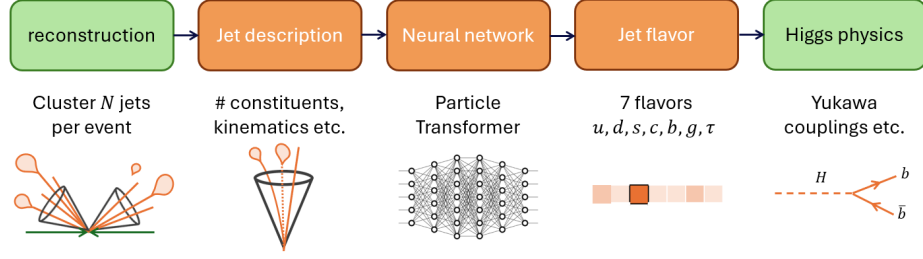


Fig. 1: Graphical illustration of the jet-flavor tagging set-up. First, jets get clustered with the anti- k_t algorithm. We describe jets by characterizing their constituents. This description serves as input to a neural network, the Particle Transformer. It performs a jet-based classification task on 7 labels representing the 7 Higgs decay channels. Jet-flavor tagging is crucial for the FCC-ee physics program. In this work, we discuss the jet description, the network and the flavor-tagging performance highlighted in orange.

The jet-flavor tagging set-up is graphically illustrated in Figure 1. After reconstructing detector signals to particle signatures such as tracks and showers, this information is used by the pandora framework [2] to form Particle Flow Objects (PFOs) which are a holistic description of a particle traveling through a detector. The jet-clustering algorithm, in our case exclusive anti- k_t [3], takes PFOs as an input to build jets. Every jet is therefore described by its constituents which are characterized by their kinematics, particle identification (PID) or, if charged, track parameters. How tracking is done at FCC-ee is summarized in the Appendix 5.1. We describe the jet constituents in detail in Section 1.4 as they serve as input features to the neural network, in our case the Particle Transformer [4]. It performs a classification task on seven labels which represent the possible Higgs decay channels into u , d , c , s , b , g and τ or their respective antiparticles. The differentiation between these channels is crucial for the FCC-ee physics program.

1.2 Theoretical background to jet-tagging

To be able to distinguish each flavor (u , d , c , s , b , g and τ) from each other, we must understand the differences in jet characteristics emerging from these particles. The τ -jet has a significantly different jet structure compared to the quarks as the τ is a lepton and only produces micro-jets by its predominant hadronic decay channels. This is especially reflected in a lower number of jet constituents compared to all other flavors. Heavy quarks (b , c) also have a characteristic property. They form long-lived mesons that travel a macroscopic distance before decaying and produce secondary vertices. These vertices are displaced from the interaction point. Accurate track fitting provides information on these displacements and so-called impact parameters (IP) can be defined to characterize displaced tracks. b -jets have further and more displaced tracks than c -jets. Lighter quarks such as u , d and s do not contain displaced tracks in their jets. s -jets can only be distinguished from u - and d -jets with PID of charged hadrons as

more hadrons with s -quark content are formed. A jet generally contains mostly pions and some kaons which appear in higher multiplicity in s -jets. As gluons (g) carry a larger color charge than quarks, they tend to have larger particle multiplicities. Due to a softer fragmentation function of gluons compared to hadrons, the jet momentum is distributed over more particles whereas quark-jets often have an energetically leading particle [1].

1.3 Detector simulations at FCC-ee

Fast simulations aim to mimic key features of a detector’s response being time and computationally efficient. Therefore, it is well suited for early feasibility studies. DELPHES [5] is the fast simulation tool used for FCC-ee, especially describing the proposed IDEA detector [6]. To study the CLD detector in fast simulation for jet-flavor tagging, we modify the extensively tested DELPHES card normally used for IDEA and exchange the tracking system to a silicon track detector with the same geometry and resolutions as in the CLD full simulation. This setup is referred to as ”CLD fast simulation” in the following. This assumption is justified in Section 2.2.

Full simulation on the other hand models every detector part and particle interactions considering all physics processes in great detail. This simulation should match the quality of real data. Out of the proposed detectors at FCC-ee, CLD has the most advanced full simulation implementation and reconstruction chain. The detector geometry is simulated with GEANT4 and the reconstruction is implemented via the MARLIN-framework [7].

Considering jet-flavor tagging, the difference between IDEA and CLD breaks down to the determination of PID. While IDEA has a drift chamber to extract time-of-flight (ToF) and cluster counting (dN/dx) information to distinguish hadrons types, CLD has no dedicated detector to extract PID.

1.4 Network architecture, input features and training

Due to the complex nature of hadronization, deep learning has become the standard approach for jet-flavor tagging. Some network architectures are explicitly developed for tagging. We use one of these state-of-the-art architectures, the Particle Transformer (ParT) [4]. We allow up to 75 particles per jet as an input to the network. Each of these particles is described with 33 input parameters at CLD and with the addition of dN/dx and ToF 35 input parameters at IDEA. The description of the jet constituents includes kinematic variables, PID and track properties for charged particles. If particles are neutral and therefore do not have tracks, the track variables are set to a dummy value lying outside the distribution. An overview of the parameters used for the training can be seen in Table 1.

The network is trained on a classification problem for the seven different Higgs decay channels. If not stated otherwise, we use a total of two million jets per flavor of which 190k are used for training and 100k for evaluation.

Variable type	Description	Number of parameters
Kinematics	$\log E_{\text{rel}}, \theta_{\text{rel}}, \phi_{\text{rel}}$	3
Identification	reco PID, charge, PID flags	7
Track displacements	d_0, z_0 , covariance matrix c_{ij} SIP in 2D and 3D (& significance), jet-track distance d_{3D} (& significance)	23

Table 1: Overview of the 33 input parameters used for training ParT on CLD. IDEA has two additional inputs: dN/dx and ToF. For a thorough description see [1].

2 Jet-flavor tagging in fast simulation

2.1 CLD vs. IDEA

Jet-flavor tagging at IDEA was previously studied in fast simulation using a different network architecture, ParticleNet [8]. To verify performance and compare with CLD, we train ParT separately on IDEA and CLD fast simulations. The results of the study are shown in Figure 2.

The receiver operating characteristic (ROC) curves show the jet misidentification probability (false positive rate) in logarithmic scale against the jet tagging efficiency (true positive rate). We present the results of this multi-class problem as a binary pairwise comparison of the classes. Therefore, we normalize the predicted probabilities of the two classes of interests over the two classes. Using b - vs. c -tagging as an example, we built the ROC curves from $D_b = \frac{P(b)}{P(b)+P(c)}$ and $D_c = \frac{P(c)}{P(b)+P(c)}$. For a smoother binning, we use $\log_{10} \frac{D}{1-D}$. The closer the curves are to the right lower corner, the better the results.

We can reproduce the performance of IDEA with ParT previously shown with ParticleNet[1]. The expected differences in tagging performance between CLD and IDEA due to the additional PID information at IDEA are also observed. IDEA can outperform CLD on s -tagging as well as on c - vs. ud -tagging. An alternative illustration of the tagging performance is shown in the Appendix, Figure 14. We plot the non-binary discriminates as $\log \frac{p_i}{1-p_i}$ with p_i being the probabilities for a class $i \in ud, s, c, b, g, \tau$. ud refers to the average probability of u and d . The more separated the distributions of the classes to the distribution of the class of interest, the better the result. Again, we see that the s -tagging discriminates are more entangled at CLD than at IDEA leading to worse separation between ud - and s -jets. Without the PID information of hadrons, s -jets are nondistinguishable from first-generation jets.

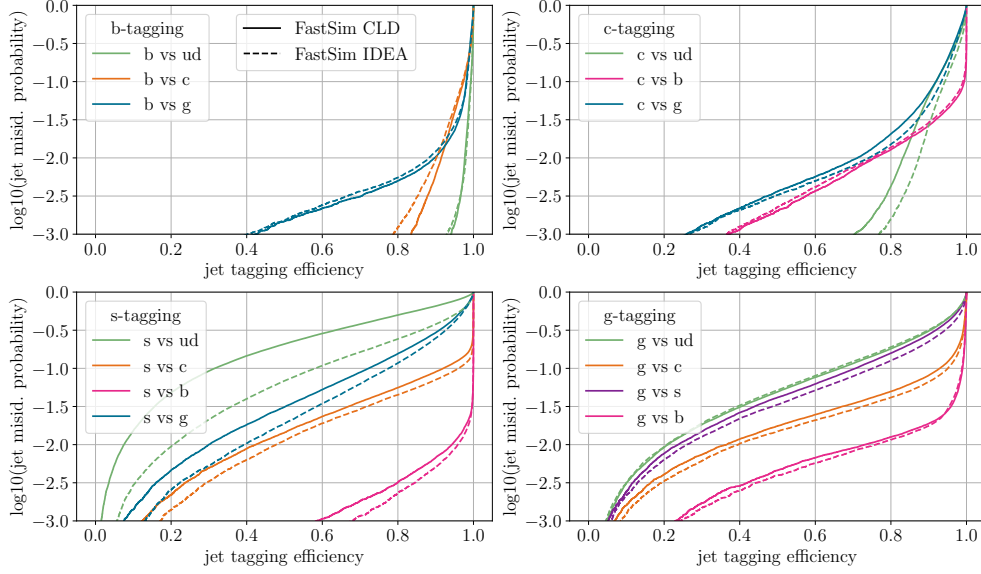


Fig. 2: ROC curves for b -, c -, s - and g -tagging (from upper left to lower right). The jet misidentification probability for other particles vs. the tagged particle (false positive rate) is shown as a function of efficiency (true positive rate). The solid (dashed) line shows fast simulation CLD (IDEA) results at 240 GeV. The closer the curves are to the right lower corner, the better the results.

2.2 Influence of calorimetric energy resolution

To justify the CLD fast simulation set-up that only uses a modified IDEA DELPHES card with an exchanged tracking system, we study the influence of the energy resolution of the unchanged calorimetric system on the tagging results. Therefore, we train another modified version of the IDEA detector with worse HCAL resolution simulating the CMS detector at LHC using the exact same training setup. The results can be seen in Figure 3. The difference in the tagging performance due to the worse HCAL resolution seems negligible, only a small deviation on s vs. ud is visible.

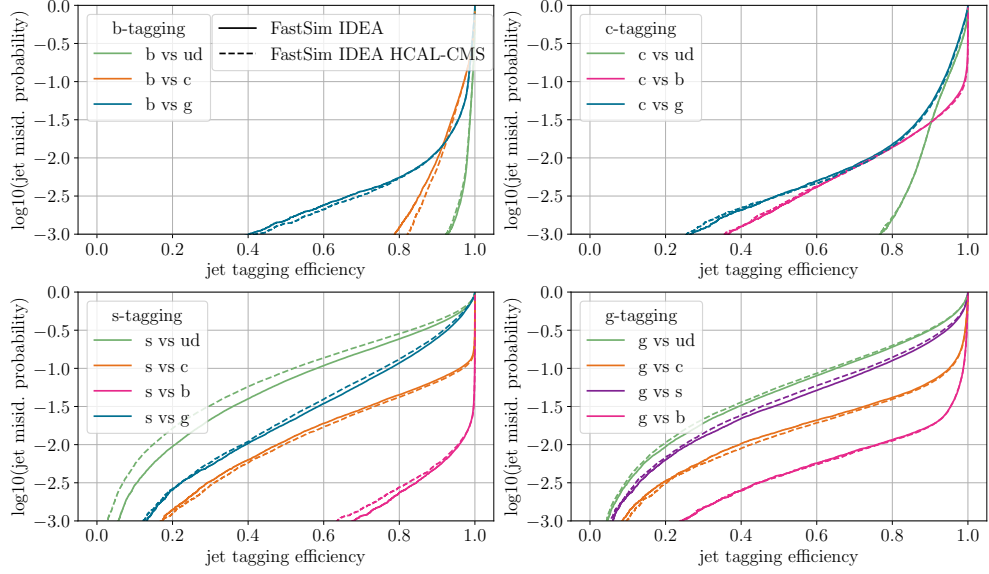


Fig. 3: Tagging performance as ROC curves of IDEA fast simulation at 240 GeV with dual readout calorimeter (solid line) and CMS HCAL resolution (dashed line). The closer the curves are to the right lower corner, the better the results.

3 Jet tagging observables in full simulation at CLD

The performance of ParT is limited by the quality of the input data. To implement jet-flavor tagging on full simulation, we must examine and understand the input features of the neural network first. Therefore, we perform a thorough investigation of the CLD full simulation data.

3.1 Comparison of jet observables for all Higgs channels

For a first impression of the full simulation input features, we plot their distributions for the seven discussed Higgs decay channels ($H \rightarrow u\bar{u}$, $H \rightarrow d\bar{d}$, $H \rightarrow c\bar{c}$, $H \rightarrow s\bar{s}$, $H \rightarrow b\bar{b}$, $H \rightarrow gg$, $H \rightarrow \tau^-\tau^+$). The observables demonstrate consistent agreement among the different channels. As expected, the particle multiplicities in jets plotted in Figure 4a show very small particle multiplicities for τ -jets and the highest particle multiplicity for gluon jets. The significance of the signed IP in 2D in Figure 4b shows the expected asymmetry from left to right in the case of b and c quarks that originates from secondary vertices of long-lived mesons.

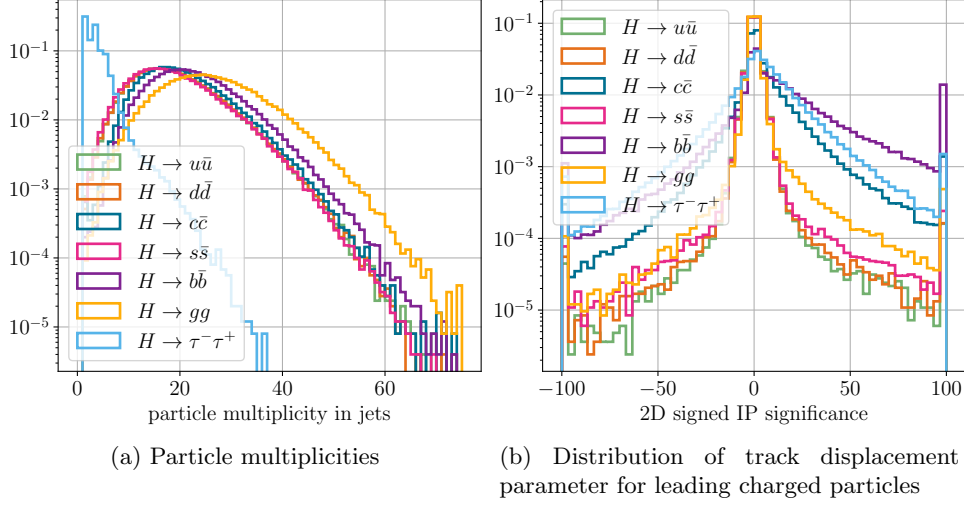


Fig. 4: Comparison of different Higgs decay channels in CLD full simulation using 250 jets.

3.2 Comparison of jet observables in fast and full simulation for $H \rightarrow b\bar{b}$

To understand the jet constituent observables in full simulation in more detail, we compare them to fast simulation. Exemplary, we choose the dominant Higgs decay channel $H \rightarrow b\bar{b}$.

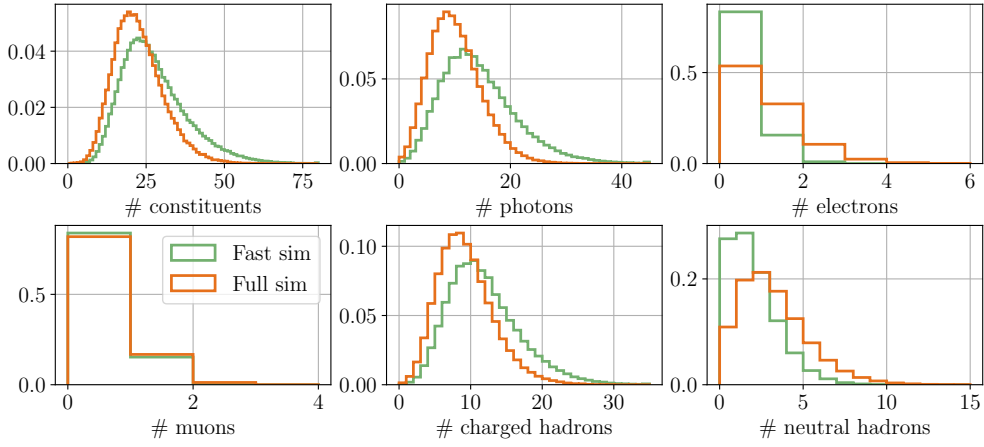


Fig. 5: Distributions of jet-constituent multiplicities in fast (green) and full (orange) simulation using 250k $H \rightarrow b\bar{b}$ jets.

Figure 5 shows the multiplicity of all particles and specific particle types in jets in fast and full simulation. As expected, jets contain mostly photons emerging from the neutral pion decay and charged hadrons (pions, kaons). Full simulation shows an overall lower multiplicity of particles in jets. We want to highlight that there are more neutral but less charged hadrons in full simulation. We are particularly interested in comparing the observables of the jet constituents as they define the characteristics of a jet. We can describe them with kinematic observables, their identification and, if charged, with track characteristics. Most of the compared jet observables in our study are in good agreement. As an example, we show the longitudinal impact parameter z_0 for the leading order charged particles in Figure 6a. The distributions including the tails match. Other track displacement observables for $H \rightarrow u\bar{u}$, $H \rightarrow c\bar{c}$ and $H \rightarrow g\bar{g}$ comparing fast and full simulation at CLD are shown in the Appendix, Figure 15.

We note that the description of tracks in full simulation is still missing the shift of the primary vertex to the true interaction point. We manually apply the shift to all parameters of the helix but the relative angles and the covariance matrix as done in fast simulation.

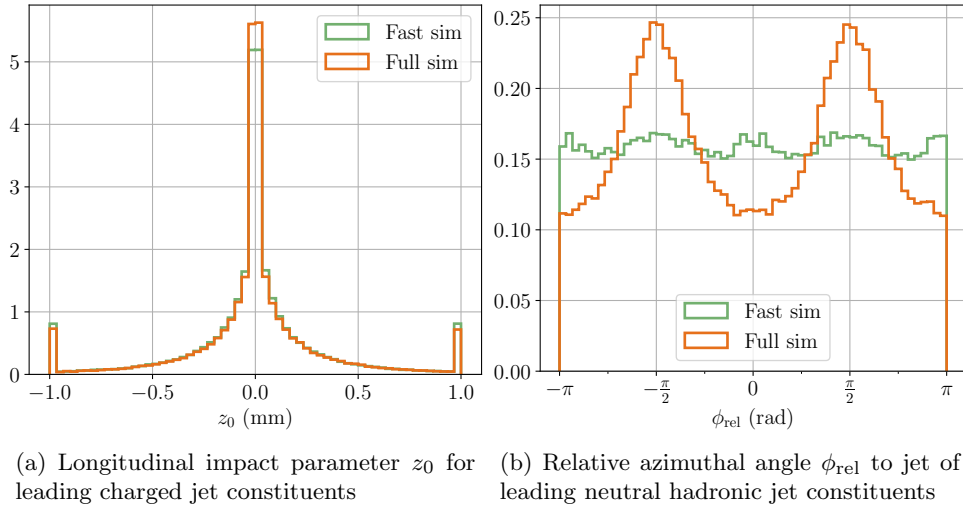


Fig. 6: Distributions of jet constituent observables in full (orange) and fast (green) simulation using 250k $H \rightarrow b\bar{b}$ jets.

3.3 Analysis of key problems in full simulation

Two major problems arise in full simulation compared to fast simulation: fake neutrals and lost tracks.

3.3.1 Fake neutrals

The main difference observed through analyzing the distributions of jet-constituent observables is the creation of fake neutral hadrons in full simulations. It becomes

apparent when examining the relative azimuthal angle ϕ between the jet and its components. The distribution of ϕ_{rel} is expected to be flat, as we observe in fast simulation and for charged jet constituents in full simulation. The distribution of ϕ_{rel} for neutral particles in full simulation is not flat but shows smeared-out peaks around $\pm\frac{\pi}{2}$, see Figure 6b. It can be mathematically derived that if the jet and its constituents have similar angles in θ and ϕ , then ϕ_{rel} approaches $\pm\frac{\pi}{2}$. High energetic charged particles leave large showers in the calorimeter. Such a large shower might get wrongly split into two, one high-energetic shower associated with the track and one less energetic shower. The less energetic shower without a track will be falsely reconstructed as a neutral particle. The problem is sketched in Figure 7. A fake neutral will have similar angles as the original charged particle. As high-energetic charged particles often dominate the jet kinematics, the jet and the fake neutral have similar angles too. In this case $\phi_{\text{rel}} \rightarrow \pm\frac{\pi}{2}$ which we observe in the data. Other analyses seem to face the same problem of fake neutral creation in pandora [9].

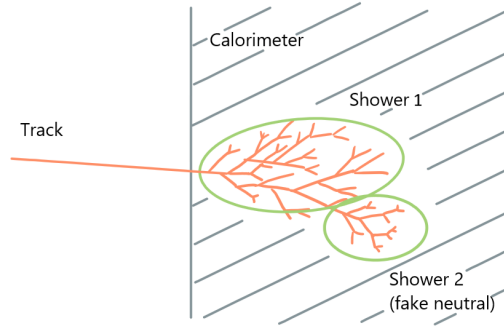


Fig. 7: Sketch of fake neutral reconstruction. A high-energetic charged particle leaves a track and a large shower in the calorimeter. The shower is split in two of which one has no track associated and is therefore reconstructed as a fake neutral.

3.3.2 Lost tracks

Pandora matches tracking information and clustering information from calorimetry to form reconstructed particles as PFOs. Neutral particles only contain calorimetric shower information as they do not leave tracks while charged particles are built from tracking and shower (cluster) information. A possible bottleneck for the performance of the network in full simulation is lost charged particles. As tracks are more relevant for jet-flavor tagging due to the unique track displacements for different flavors, we might lose important information. Therefore, we investigate the performance of reconstructing charged PFOs in full simulation.

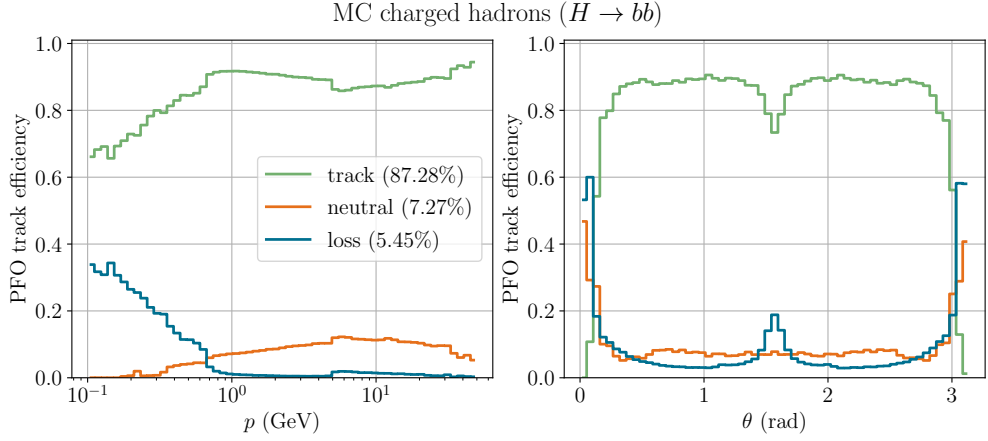


Fig. 8: MC charged hadrons from full simulation $H \rightarrow b\bar{b}$ events shown as a fraction of which are reconstructed with track (green), reconstructed as neutral (orange) or not reconstructed at all (blue) as a function of MC momentum p (left) and MC polar angle θ (right).

Considering all charged MC particles that leave at least four tracker hits, we check whether there is a reconstructed particle associated that uses at least 30 % of the MC tracker hits or MC calorimeter cluster hits. If there is no such reconstructed particle, we mark it as lost. Otherwise, we check if an associated track got reconstructed using at least 30 % of the MC tracker hits. If so, we mark the particle as reconstructed with track, otherwise, it is marked as neutral. The results of that study are exemplary shown in Figure 8 for charged hadrons of the $H \rightarrow b\bar{b}$ channel. We see the fraction of MC charged hadrons that got reconstructed with track information (green), reconstructed without track information (orange) and not reconstructed (blue) as a function of MC momentum p (left) and MC polar angle θ (right). The efficiency of reconstructing tracks rises with increasing momentum until 1 GeV while fewer tracks get lost. There is a clear drop in the performance at $p = 5$ GeV which originates from the pandora reconstruction. Above 5 GeV the algorithm requires a track to point toward a cluster to be used to reconstruct a charged particle as it assumes that the energy of the particle is high enough to reach the calorimeter. The additional constraint causes MC-charged particles to get lost or wrongly reconstructed as neutrals because unmatched tracks get lost. Furthermore, we see a loss of charged particles perpendicular to the beam line. These are particles that move on spiraling paths in the magnetic field never reaching the calorimeter. These are probably marked as lost as they leave many hits in the tracker which are not all used for reconstruction and therefore do not fulfill the selection requirement of 30 % used tracker hits.

4 Jet-flavor tagging in full simulation at CLD

4.1 Results and comparison to fast simulation

We perform a training of the ParT on full simulation CLD with the same training set-up as in fast simulation. The results and the comparison to fast simulation are shown in Figure 9 as ROC curves. Again, the closer the curves are to the right lower corner, the better the results. As expected, tagging on full simulation does not reach the performance of tagging in fast simulation with the current reconstruction problems explained in Section 3.3. Taking c -tagging as an example, the efficiency of c vs. ud drops from over 80 % to under 70 % at a misidentification probability of 10^{-2} .

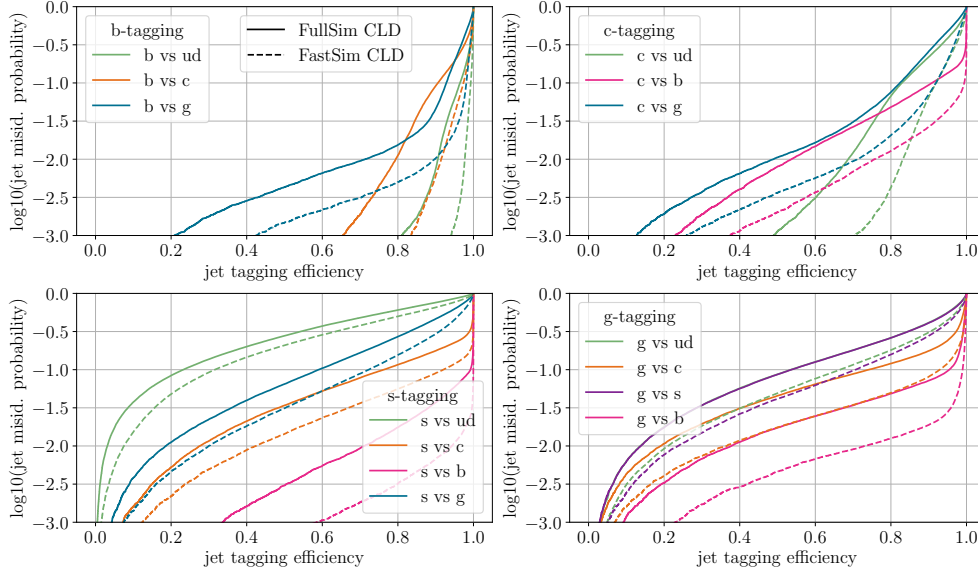


Fig. 9: ROC curves for b -, c -, s - and g -tagging (from upper left to lower right). The jet misidentification probability for other particles vs. the tagged particle is shown as a function of efficiency. The solid (dashed) line shows full (fast) simulation CLD results at 240 GeV. The closer the curves are to the lower-right corner, the better the results.

4.2 Results using complete track information

To investigate whether the missing tracks (via loss or neutral PFO reconstruction) described in Section 3.3.2 indeed affect the jet-flavor tagging results, we introduce a workaround of the problems that simulates an improved pandora particle-flow algorithm. To not lose tracks, we retrieve charged particles by considering all reconstructed tracks (not PFOs) and match them via their polar angle to the two jets in the events. We use the MC PID for charged particles to classify them as electrons, muons or charged hadrons to maintain the same input features to the network as when using PFOs. Neutral particles are retrieved by considering neutral PFOs in the jets while

checking their MC PID to be neutral to not double-count charged particles. With this method, we also avoid the problem of fake neutral particles described in Section 3.3.1.

Figure 10 shows the results (dashed lines) labeled as "track-based full simulation CLD" highlighting that information about charged particles is retrieved from tracks and not PFOs. We compare the results to the full simulation CLD tagging performance (solid lines) from Section 4.1 that is purely based on PFO information. The ROC curves suggest that using complete track information leads to a significant improvement in the tagging performance. Taking b -tagging as an example, the tagging efficiency for b vs. ud quarks for a 10^{-2} misidentification probability rises from 90 % to 95 %.

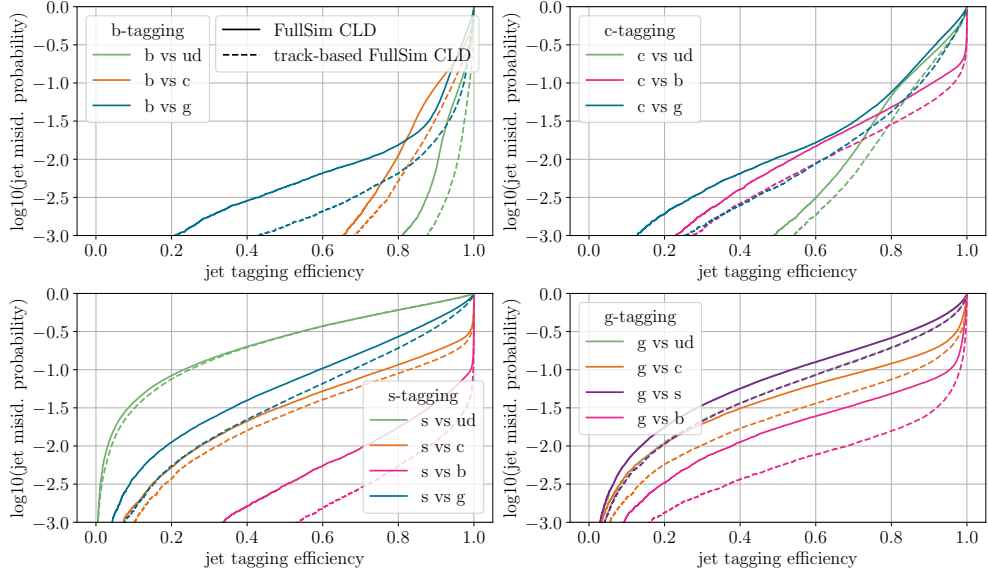


Fig. 10: ROC curves for b -, c -, s - and g -tagging (from upper left to lower right). The jet misidentification probability for other particles vs. the tagged particle is shown as a function of efficiency. The solid line shows full simulation CLD results at 240 GeV using PFOs. The dashed line corrects the reconstruction by considering all reconstructed tracks instead of charged PFOs and tests the PID of neutral PFOs to avoid double counting.

In the Appendix, we show the ROC curves for fast simulation vs. this track-based full simulation approach in Figure 16. In Figure 11, we show the tagging performance as non-binary discriminates as $\log \frac{p_i}{1-p_i}$. The more separated the distributions of the classes to the distribution of the class of interest, the better the result. Some more uncommon discriminants for s -, u - and τ -tagging can be seen in the Appendix, Figure 17 as well as some uncommon ROC curves showing u -, d - and τ -tagging in the Appendix, Figure 18.

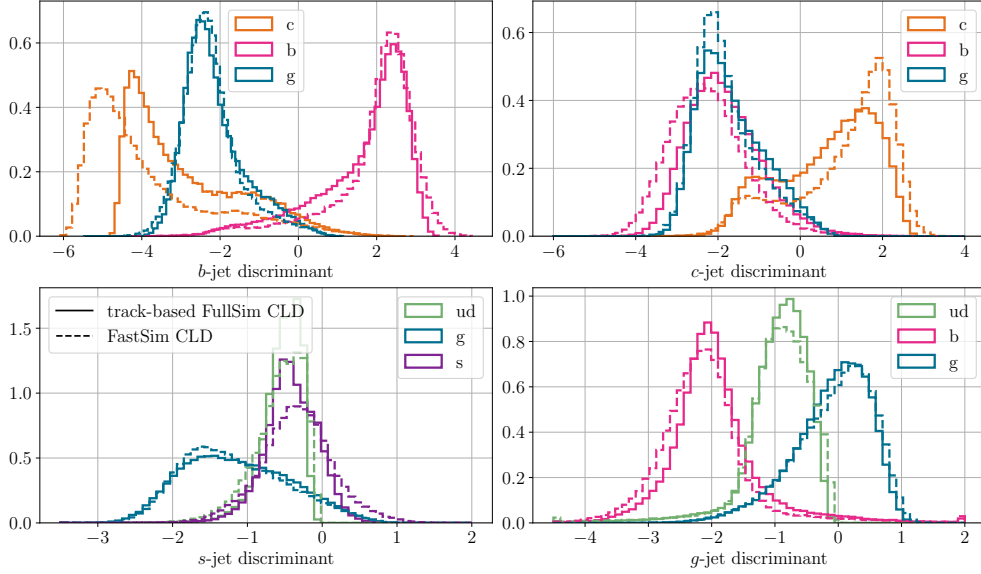


Fig. 11: Tagging performance of track-based full simulation CLD (solid line) vs. fast simulation CLD (dashed line) showing the discriminates as $\log \frac{p_i}{1-p_i}$. *ud* refers to the average probability of *u* and *d*.

4.3 Results using tracks only

In Section 4.2 we showed that using all available tracks for tagging boosts the performance. However, we used some MC information to perform the correction on full simulation. Therefore, we investigate if using track information only which does not require to use of MC information still outperforms the PFO-based full simulation tagging performance.

The results of this study can be seen in Figure 12. We compare the pandora full simulation performance (solid line), the track-based pandora-corrected full simulation performance (dashed line) and the full simulation performance using tracks only (dotted line). Using tracks only is not as good as using the track-based pandora correction but also better than the current pandora performance. In *b*-tagging, using tracks seems to be an appropriate approach while *s*- vs. *ud*-tagging or *c*- vs. *ud*-tagging suffers from the loss of information about neutrals. Using tracks only might be a valid short-term solution for *b*-tagging but to achieve an overall outstanding tagging performance, the CLD community should focus on an improved particle-flow algorithm with pandora.

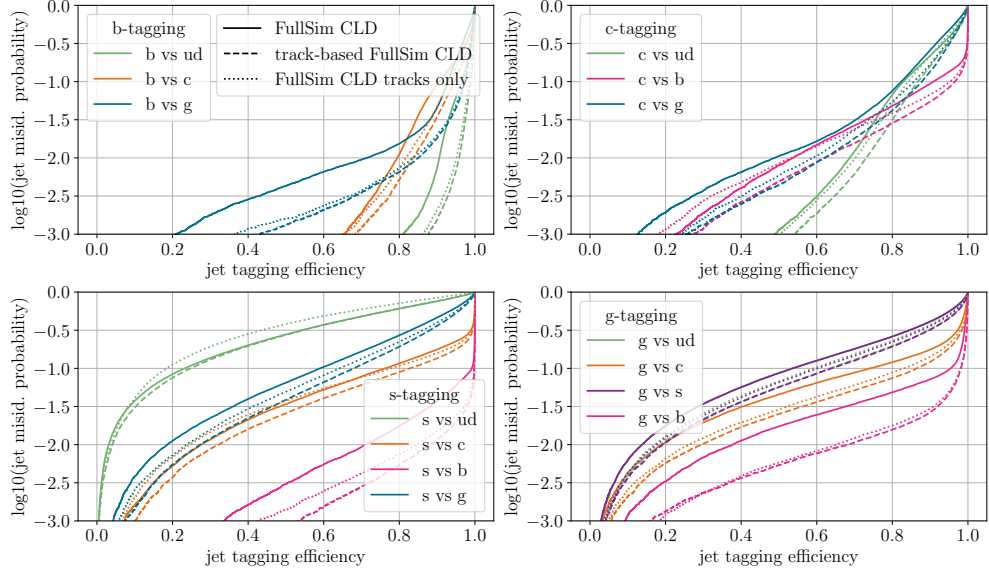


Fig. 12: Tagging performance of full simulation CLD using tracks only (solid line) vs. full simulation CLD (dashed line) and the track-based full simulation CLD that corrects pandora flaws (dotted line) as ROC curves.

For this study, we did not use MC information. We can retrieve all network input features, see Tabular 1, from the track information apart from the PID. If a PFO is associated with the track, then its PID is used, otherwise, a dummy value is set. We investigate the influence of the PID parameter to the tagging performance, see Appendix Figure 19. Distinguishing between electrons, muons and charged hadrons seems to have a minor impact, mostly influencing *c*-tagging.

4.4 Results with secondary vertex information

Until now, we have only considered basic track information for tagging in full simulation. Although CLD does not have the capabilities to perform PID like IDEA, we can provide vertex information retrieved from tracking algorithms. Therefore, we retrain the tagger on full simulation CLD data but with added vertex position information (x, y, z) and invariant mass of the vertices. We consider V^0 s and secondary vertices for this purpose. The distribution of the invariant mass for V^0 and transverse radius for secondary vertices can be seen in the Appendix, Figure 20. The V^0 invariant mass distribution shows a clear peak at the K^0 mass of 497.6 MeV. The radius distribution of secondary vertices shows more displaced tracks for *b*-jets characterized through the longer tail similar to Figure 4b. The first two tracker layers leave noise in the distribution.

The performance does not improve using vertex information, see Figure 13. The performance fluctuates around the standard full simulation CLD performance instead.

This indicates that the network can learn vertexing on its own through track displacements and track kinematics so that the added vertex information does not add valuable information to the network.

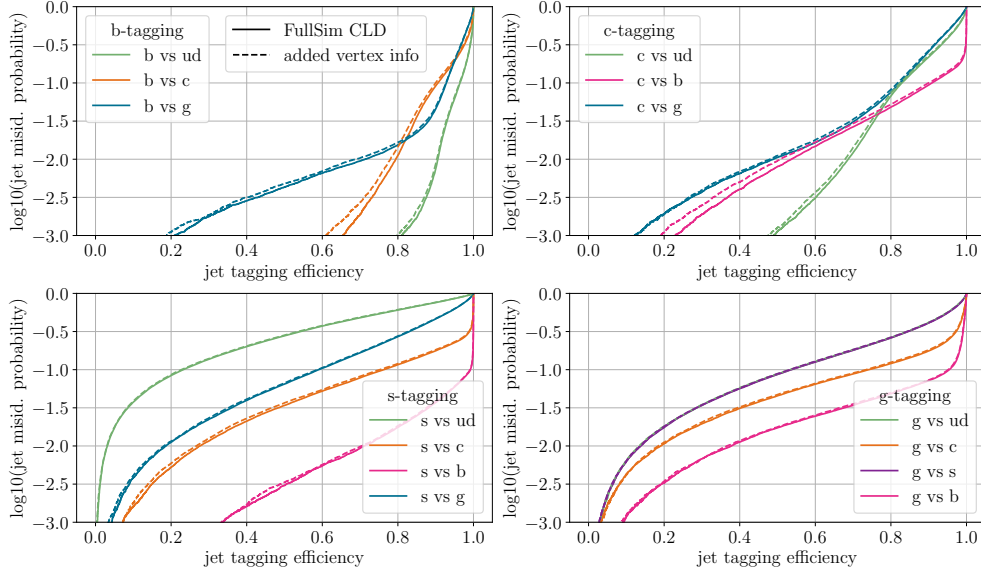


Fig. 13: Tagging performance of CLD full simulation at 250 GeV without (solid line) and with (dashed line) vertex information (invariant mass and coordinates of V^0 s and secondary vertices).

5 Summary and Discussion

We study the performance of jet-flavor tagging at the CLD and IDEA detector at 240 GeV in fast simulation using transformer-based machine learning. While we can reproduce the previously shown tagging performance at IDEA, we study the influence of PID by performing jet-tagging on CLD. As expected, especially s -tagging and c -vs. ud -tagging suffer from the lack of PID information at CLD compared to IDEA.

We present the first study of jet-flavor tagging on full simulation at CLD at 240 GeV. When comparing the results to fast simulation, the first results in full simulation do not yet achieve the same level of performance. Full simulation jet-flavor tagging improves if tracks are used instead of charged PFOs as mistakes in the reconstruction chain such as lost tracks or fake neutral particles are avoided. This encourages future work on the CLD reconstruction for more precise physics analysis. A short-term alternative, especially for b -tagging, is the usage of tracks instead of PFOs for jet-tagging.

Although CLD has no dedicated detector for Time-of-Flight (ToF) or dN/dx measurements, dE/dx information could be retrieved from the silicon trackers. In the past,

these measurements have not been considered sufficiently precise for PID but might provide valuable information for tagging with machine learning methods. Leveraging dE/dx might further push the limits of jet-flavor tagging at CLD. The CLD-community might envisage a RICH detector in the future which could provide similar PID capabilities as dN/dx at IDEA. Although s -tagging will improve with this setup, the overall tagging performance might suffer due to more detector material influencing the crucial particle flow performance.

Acknowledgements

This work has been partly supported by the Future Circular Collider Innovation Study (FCCIS) project, that has received funding from the European Union’s Horizon 2020 research and innovation programme under grant No 951754.

References

- [1] F. Bedeschi, L. Gouskos, M. Selvaggi, Jet flavour tagging for future colliders with fast simulation. *The European Physical Journal C* **82**(7) (2022). <https://doi.org/10.1140/epjc/s10052-022-10609-1>. URL <http://dx.doi.org/10.1140/epjc/s10052-022-10609-1>
- [2] J.S. Marshall, M.A. Thomson. The pandora particle flow algorithm (2013). URL <https://arxiv.org/abs/1308.4537>
- [3] M. Cacciari, G.P. Salam, G. Soyez, The anti-ktjet clustering algorithm. *Journal of High Energy Physics* **2008**(04), 063–063 (2008). <https://doi.org/10.1088/1126-6708/2008/04/063>. URL <http://dx.doi.org/10.1088/1126-6708/2008/04/063>
- [4] H. Qu, C. Li, S. Qian. Particle transformer for jet tagging (2024). URL <https://arxiv.org/abs/2202.03772>
- [5] J. de Favereau, C. Delaere, P. Demin, A. Giammanco, V. Lemaître, A. Mertens, M. Selvaggi, Delphes 3: a modular framework for fast simulation of a generic collider experiment. *Journal of High Energy Physics* **2014**(2) (2014). [https://doi.org/10.1007/jhep02\(2014\)057](https://doi.org/10.1007/jhep02(2014)057). URL [http://dx.doi.org/10.1007/JHEP02\(2014\)057](http://dx.doi.org/10.1007/JHEP02(2014)057)
- [6] F. Bedeschi, A detector concept proposal for a circular e+e- collider. *PoS ICHEP2020*, 819 (2021). <https://doi.org/10.22323/1.390.0819>
- [7] N. Bacchetta, J.J. Blaising, E. Brondolin, M. Dam, D. Dannheim, K. Elsener, D. Hynds, P. Janot, A.M. Kolano, E. Leogrande, L. Linssen, A. Nürnberg, E.F. Perez, M. Petrič, P. Roloff, A. Sailer, N. Siegrist, O. Viazlo, G.G. Voutsinas, M.A. Weber. Cld – a detector concept for the fcc-ee (2019). URL <https://arxiv.org/abs/1911.12230>

- [8] H. Qu, L. Gouskos, Jet tagging via particle clouds. *Physical Review D* **101**(5) (2020). <https://doi.org/10.1103/physrevd.101.056019>. URL <http://dx.doi.org/10.1103/PhysRevD.101.056019>
- [9] D. Jeans, K. Yumino. Ild benchmark: a study of $e^-e^+ \rightarrow \tau^-\tau^+$ at 500 gev (2020). URL <https://arxiv.org/abs/1912.08403>
- [10] E. Brondolin, E. Leogrande, D. Hynds, F. Gaede, M. Petrič, A. Sailer, R. Simoniello, Conformal tracking for all-silicon trackers at future electron–positron colliders. *Nuclear Instruments and Methods in Physics Research Section A: Accelerators, Spectrometers, Detectors and Associated Equipment* **956**, 163304 (2020). <https://doi.org/10.1016/j.nima.2019.163304>. URL <http://dx.doi.org/10.1016/j.nima.2019.163304>

Appendix

5.1 Track reconstruction in fast and full simulation

As tracking is responsible for reconstructing charged particles, it is of great importance for jet flavor tagging. Therefore, we summarize the track reconstruction methods used in fast and full simulation at FCC-ee.

DELPHES [5] performs a fast simulation of the tracking performance for detectors at FCC-ee [1]. It describes two tracking system geometries: cylinders coaxial to the beam direction and planar disks orthogonal to the beam direction. Strip, wire and pixel measurement geometries are included in the framework. Each layer of the tracking system geometry describes either a measurement or accounts as passive material contributing to multiple scattering. As tracking is performed in a magnetic field, charged particles move on a helix trajectory. Therefore, the track can be described with five parameters $\vec{\alpha}$. To reconstruct the track parameters $\vec{\alpha}$ from measured coordinates \vec{d}^* , a χ^2 minimization with respect to the track parameters $\vec{\alpha}$ is performed:

$$\chi^2 = (\vec{d} - \vec{d}^*)^t S^{-1} (\vec{d}^* - \vec{d}) \quad (1)$$

where \vec{d} are the predicted coordinates derived from $\vec{\alpha}$ and the geometry of each measurement layer. S is the covariance matrix of all measurements including detector resolutions and multiple scattering [1].

Full simulation at CLD uses conformal tracking [10]. This method combines two strategies: conformal mapping and cellular automaton-based track finding. Conformal mapping transforms point coordinates in Euclidean space into the conformal space. This is useful as circles passing through the origin in Euclidean space turn into straight lines in conformal space. Therefore, the problem of helix fitting is simplified to finding straight lines in this chosen space. But in real physics processes, there are deviations from a perfect path e.g. through multiple scattering. As displaced particles do not pass through the origin, their straight line can also only be mathematically approximated. Therefore, cellular automaton is used for pattern recognition in conformal space consisting of two steps: building and extending cellular track candidates.

5.2 Additional plots

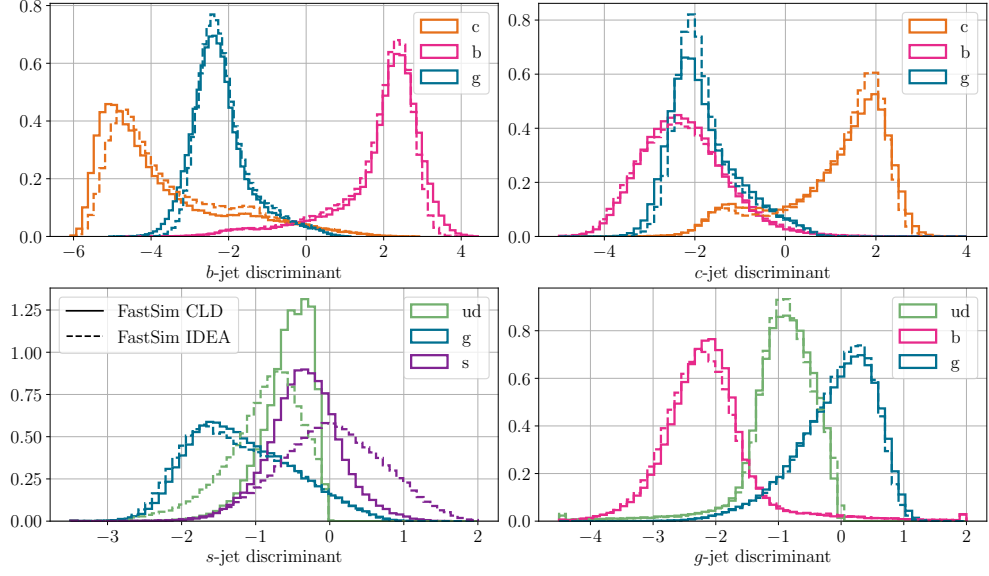


Fig. 14: Tagging performance of fast simulation CLD (solid line) vs. fast simulation IDEA (dashed line) showing the discriminates as $\log \frac{p_i}{1-p_i}$. *ud* refers to the average probability of *u* and *d*. IDEA's PID capability enables *s*- vs. *ud*-jet distinction, unlike CLD.

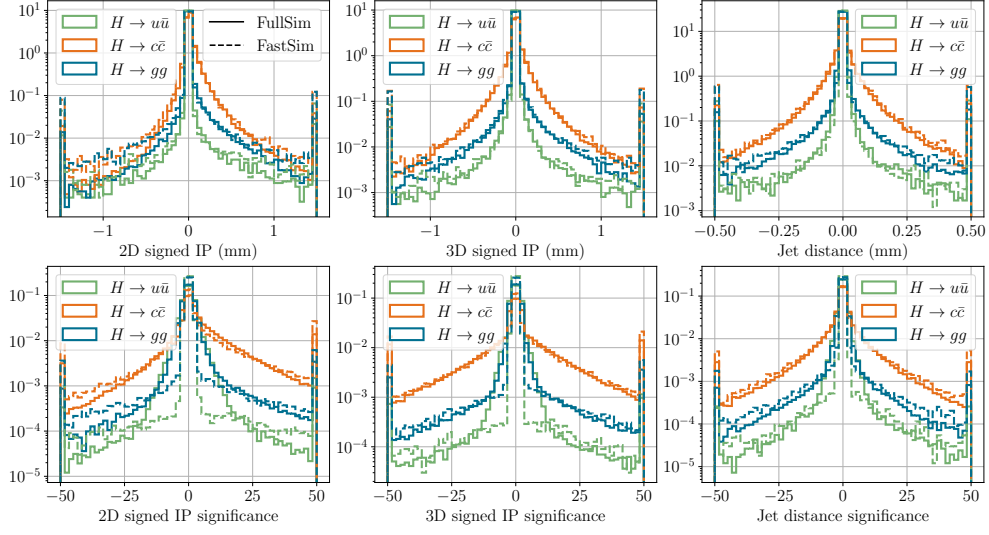


Fig. 15: 2D and 3D signed impact parameters, jet distance and their significances from leading tracks of $H \rightarrow u\bar{u}$ (green), $H \rightarrow c\bar{c}$ (orange) and $H \rightarrow g\bar{g}$ (blue) in full (fast) simulation shown as a solid (dashed) line.

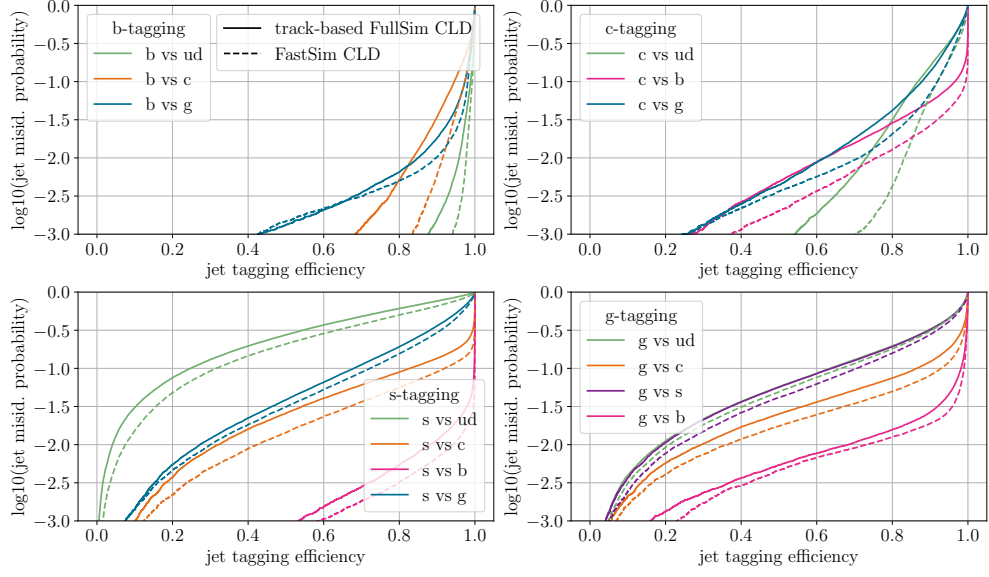


Fig. 16: ROC curves for b -, c -, s - and g -tagging (from upper left to lower right). The jet misidentification probability for other particles vs. the tagged particle is shown as a function of efficiency. The dashed line shows fast simulation CLD results at 240 GeV. The solid line shows track-based full simulation CLD results which correct the reconstruction by considering all reconstructed tracks instead of charged PFOs and tests the PID of neutral PFOs to avoid double counting.

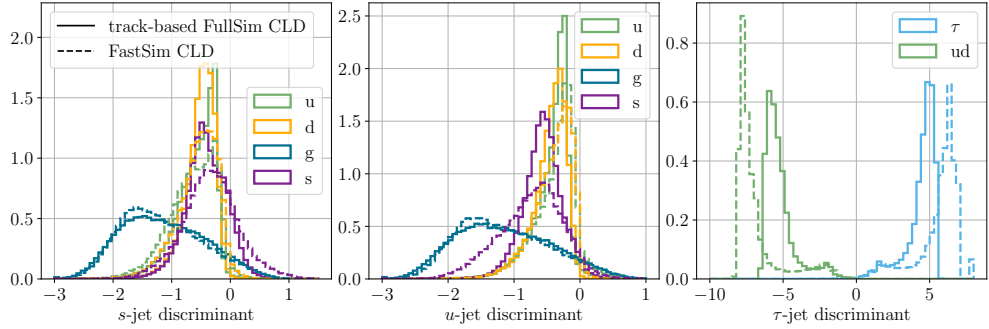


Fig. 17: Tagging performance of track-based full simulation CLD (solid line) vs. fast simulation CLD (dashed line) showing the discriminates as $\log \frac{p_i}{1-p_i}$. ud refers to the average probability of u and d .

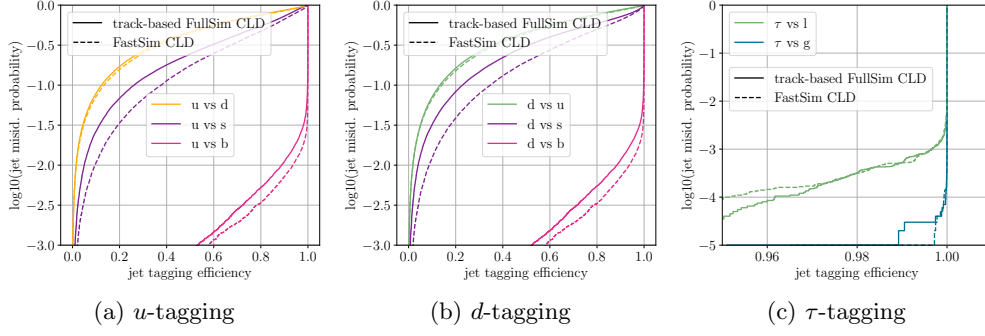


Fig. 18: ROC curves for different classes (u , d , τ from left to right) for track-based full simulation CLD (solid line) and fast simulation CLD (dashed line). The jet misidentification probability for other particles vs. the tagged particle is shown as a function of efficiency.

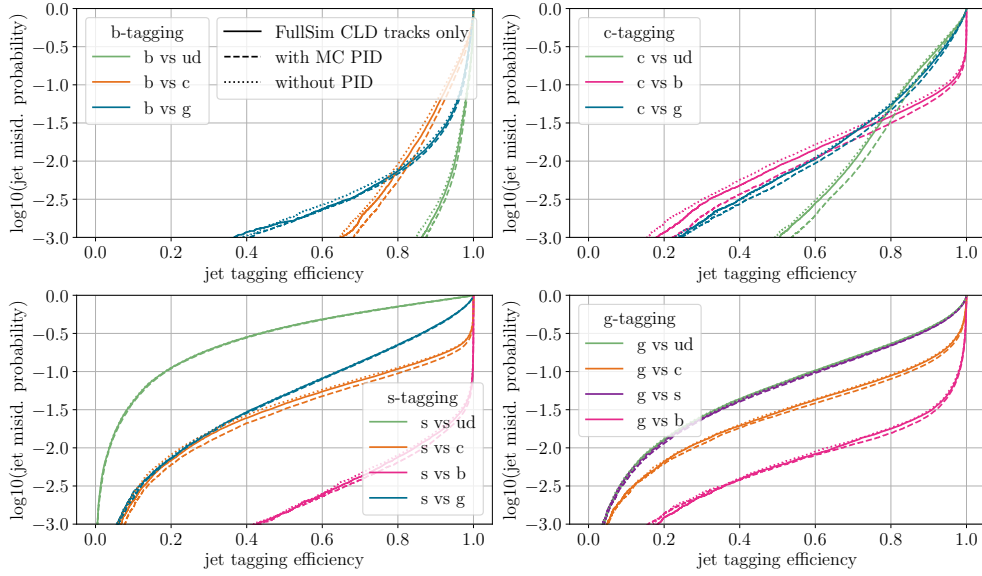


Fig. 19: Tagging performance of full simulation CLD using tracks only (solid line) shown as ROC curves. Variations of using not the reconstructed PID from PFOs but the MC PID (no PID) are shown as a dashed (dotted) line.

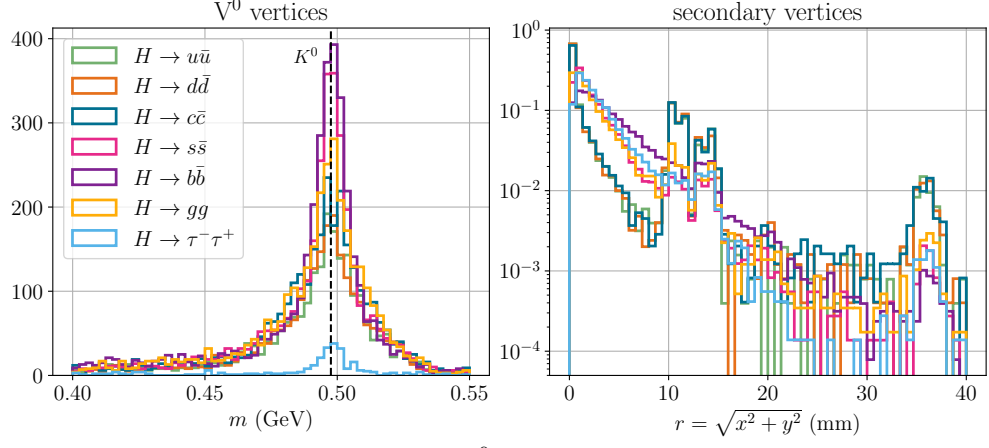


Fig. 20: Invariant-mass spectrum of V^0 (left) and transverse radius of secondary vertices (right) for different Higgs decay channels (250k jets per channel). PDG masses of relevant particles are indicated with a black dashed line.